First Order Reversal Curves for the Evaluation of Thickness Dependent Ferroelectric Switching in $Al_{0.7}Sc_{0.3}N$ Film

Subhranu Samanta
Institute of Microelectronics
*Agency for Science Technology and Research (A*STAR)*
Singapore
Subhranu_Samanta@ime.a-star.edu.sg

Chen Liu
Institute of Microelectronics
*Agency for Science Technology and Research (A*STAR)*
Singapore
liu_chen@ime.a-star.edu.sg

Zichu Wang
Institute of Microelectronics
*Agency for Science Technology and Research (A*STAR)*
Singapore
ZichuW.GE2122@tum-asia.edu.sg

Li Chen
Institute of Microelectronics
*Agency for Science Technology and Research (A*STAR)*
Singapore
chen_li@ime.a-star.edu.sg

Yao Zhu
Institute of Microelectronics
*Agency for Science Technology and Research (A*STAR)*
Singapore
zhuya@ime.a-star.edu.sg

Minghua Li
Institute of Microelectronics
*Agency for Science Technology and Research (A*STAR)*
Singapore
li_minghua@ime.a-star.edu.sg

Binni Varghese
Institute of Microelectronics
*Agency for Science Technology and Research (A*STAR)*
Singapore
Binni_Varghese@ime.a-star.edu.sg

Huamao Lin
Institute of Microelectronics
*Agency for Science Technology and Research (A*STAR)*
Singapore
Lin_Huamao@ime.a-star.edu.sg

Hock Koon Lee
Institute of Microelectronics
*Agency for Science Technology and Research (A*STAR)*
Singapore
lee_hock_koon@ime.a-star.edu.sg

***Abstract*—In this paper, the First-Order Reversal Curve (FORC) technique is employed to analyze the impact of scandium-doped aluminum nitride ($Al_{0.7}Sc_{0.3}N$) ferroelectric film thickness in sub-50 nm regime on coercive field and built-in-bias field distributions in Mo/$Al_{0.7}Sc_{0.3}N$/Mo metal-ferroelectric-metal (MFM) capacitors. From the FORC distribution, we find that switching density becomes widened and flattened in thinner $Al_{0.7}Sc_{0.3}N$ films. The coercive field increases with scaling down the $Al_{0.7}Sc_{0.3}N$ film thickness. This study will be helpful to understand the effect of $Al_{0.7}Sc_{0.3}N$ film thickness variation on ferroelectric switching for future non-volatile memory (NVM) applications.**

Keywords*— *FORC distribution, $Al_{0.7}Sc_{0.3}N$, thickness dependent, NVM

I. INTRODUCTION

Non-volatile ferroelectric random-access memory (FeRAM) devices are studied aggressively and extensively all over the world due to its CMOS back-end-of-line (BEOL) compatibility, low operational voltage, fast read/write cycle, and high endurance [1-5]. FeRAM consists of ferroelectric capacitor in the memory cell, and the data is stored by the remanent polarization (P_r) of the ferroelectric material. Several researchers have reported ferroelectric memories based on different ferroelectric materials like HZO [5], $BiFeO_3$ [6], PZT [7], $Al_{1-x}Sc_xN$ [3, 8, 9] etc. Among them, ferroelectricity in scandium-doped aluminum nitride ($Al_{1-x}Sc_xN$) film has become very attractive for the applications in next-generation ferroelectric NVMs owing to its CMOS-BEOL compatibility, low thermal budget (< 400 °C), large remnant polarization (P_r) > 80 μC/cm^2, near ideal rectangular shaped polarization-electric field (P-E) hysteresis, high $E_C \sim 2 – 6$ MV/cm) [1-3]. Previously, few reports have been made on thickness dependent ferroelectric switching in $Al_{1-x}Sc_xN$-based different MFM structures [8, 9]. We have reported multiscale modeling of $Al_{0.7}Sc_{0.3}N$-based FeRAM using 100 nm thick ferroelectric film [3]. However, the $Al_{1-x}Sc_xN$ film thickness-dependent FORC study has never been explored yet.

In this study, we have employed FORC approach to evaluate the impact of $Al_{0.7}Sc_{0.3}N$ film thickness on the ferroelectric switching in Mo/$Al_{0.7}Sc_{0.3}N$/Mo MFM structure. FORC measurements are used for the detailed analysis of the switching density (ρ^-), coercive field (E_c) and built-in-bias field (E_{bias}) distributions. Electrical result shows that FORC distribution becomes widened and flattened in the thinner $Al_{0.7}Sc_{0.3}N$ films. The core concentration of hysterons decreases with decreasing ferroelectric film thickness. On the other hand, E_c and reversal field ($|E_r|$) increase with decreased $Al_{0.7}Sc_{0.3}N$ film thickness. Moreover, our experimental result could be a guideline for further analysis of thinner $Al_{0.7}Sc_{0.3}N$ ferroelectric films in sub-30 nm regime.

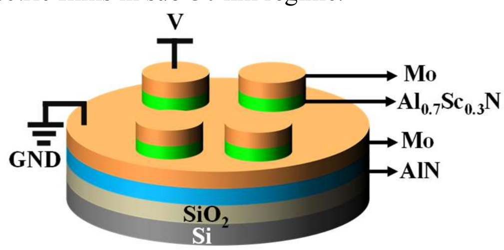

Fig. 1. Schematic of the $Al_{0.7}Sc_{0.3}N$-based MFM capacitors

TABLE I. SAMPLE SPLIT TABLE

Sample	Bottom electrode	$Al_{0.7}Sc_{0.3}N$ thickness	Top electrode
S1	Mo	50 nm	Mo
S2	Mo	40 nm	Mo
S3	Mo	30 nm	Mo

II. EXPERIMENTAL

The schematic illustration in Fig. 1 shows the structure of the $Al_{0.7}Sc_{0.3}N$-based MFM capacitor. First, 40 nm AlN seed layer followed by a 200 nm molybdenum (Mo) as bottom electrode were deposited by physical vapour deposition (PVD) process on 8-inch Si substrate. Next, $Al_{0.7}Sc_{0.3}N$ thin film was deposited by pulsed DC reactive magnetron sputtering method followed by the deposition of 100 nm Mo layer as top electrode without breaking the vacuum. A ScAl alloy target was used with the Sc:Al atomic ratio of 30:70. Three different thicknesses of 50 nm, 40 nm, and 30 nm $Al_{0.7}Sc_{0.3}N$ film were deposited. They are named S1, S2, and S3 respectively as shown in sample split Table I. Finally, lithography followed by the dry etching process were done to obtain MFM capacitors with top circular electrodes having radius of 50 µm. All the transient current (J-E) measurements are carried out by a Radiant Ferroelectric Analyzer applying triangle pulses with a frequency of 10 kHz at room temperature.

III. RESULTS AND DISCUSSION

Fig. 2 exhibits the $Al_{0.7}Sc_{0.3}N$ film thickness dependent transient current loops (J-E) measured employing FORC scheme for S1 (Fig. 2a), S2 (Fig. 2b), and S3 (Fig. 2c) MFM devices. The transient current response are recorded starting from a positive saturation field and sweeping between E_r and the positive saturation field, sequentially increasing E_r until the negative saturation field. To evaluate the impact of E_r on different thicknesses of $Al_{0.7}Sc_{0.3}N$ film in details, we have introduced ρ^- (E_r, E) which indicates the density of switchable polarization units with respect to E_r and applied electric field (E). Switching density ρ^- (E_r, E) is derived using the following formula [10]

$$\rho^-(E_r, E) = \frac{1}{2\dot{E}} \frac{\partial j^-_{FORC}(E_r, E)}{\partial E_r} \tag{1}$$

Where, $\partial j^-_{FORC}(E_r, E)$ is the difference between switching peak of two successive current density cycles in reversal field (i.e., $j^-_{FORC}(E_{r,i}, E) - j^-_{FORC}(E_{r,i-1}, E)$). Fig. 3 (a-c) shows the $Al_{0.7}Sc_{0.3}N$ film thickness-dependent distribution of ρ^- and E_r with E. The E_r distribution peak is found at - 4.7 MV/cm < E_r < - 4.6 MV/cm, - 4.85 MV/cm< E_r < - 4.68 MV/cm, and – 5.2 MV/cm < E_r < - 4.95 MV/cm for 50 nm, 40 nm, and 30 nm $Al_{0.7}Sc_{0.3}N$ films, respectively. The corresponding E peak is located at 3.82 MV/cm < E< 4.25 MV/cm, 3.9 MV/cm < E < 4.32 MV/cm, and 4.1 MV/cm < E < 4.56 MV/cm for S1, S2, and S3 respectively. It is observed that $|E_r|$ increases (S1 < S2 < S3) with scaling down the thickness of $Al_{0.7}Sc_{0.3}N$ film as shown in Fig. 3d. Interestingly, the FORC distribution becomes more widened and flattened in the thinner $Al_{0.7}Sc_{0.3}N$ films as shown in Fig.3 (a), (b), (c). The core concentration of hysterons decreases as the $Al_{0.7}Sc_{0.3}N$ film thickness decreases, whereas the switching field increases as the film thickness decreases. It is worthy to be noted that ρ^- is higher at low reversal fields E_r. This could be attributed to both domain wall (DW) oscillations and lattice intrinsic contributions at lower E_r, while at high E_r only the lattice intrinsic contribution is expected to dominate instead of DW

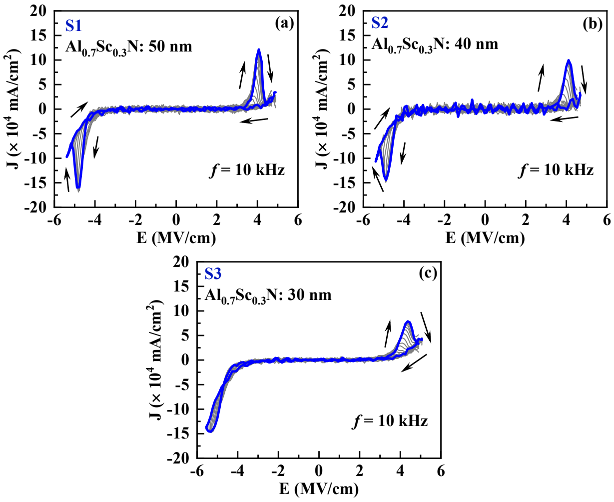

Fig. 2. Transient current loops (J-E) measured using the FORC scheme for the thickness of (a) 50 nm (S1), (b) 40 nm (S2), and (c) 30 nm (S3) $Al_{0.7}Sc_{0.3}N$ film.

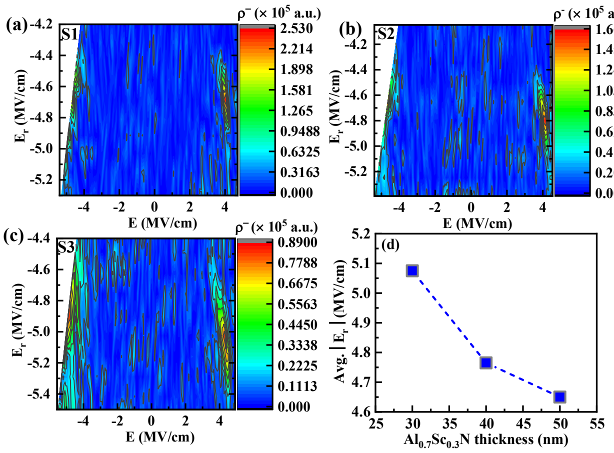

Fig. 3. Switching density (ρ^-) distribution derived from the FORC measurements (Fig.2) of $Al_{0.7}Sc_{0.3}N$ film for the thickness of (a) 50 nm (S1), (b) 40 nm (S2), and (c) 30 nm (S3). (d) Average $|E_r|$ versus $Al_{0.7}Sc_{0.3}N$ film thickness characteristics.

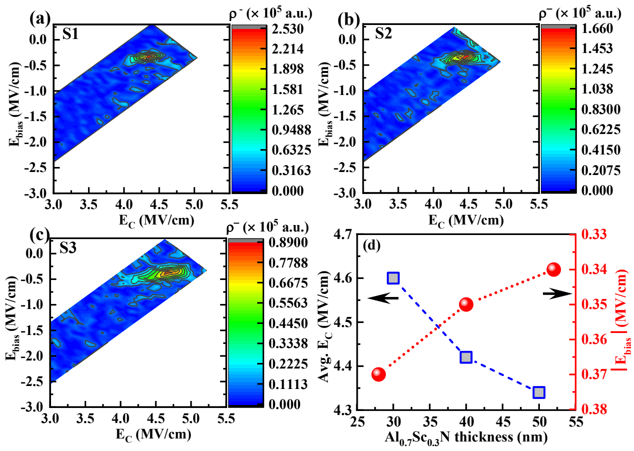

Fig. 4. Switching density (ρ^-) distribution versus built-in-bias field E_{bias}, and coercive field E_c for (a) 50 nm (S1), (b) 40 nm (S2), and (c) 30 nm (S3) $Al_{0.7}Sc_{0.3}N$ films. (d) $Al_{0.7}Sc_{0.3}N$ film thickness - dependent characteristics for average E_c and $|E_{bias}|$.

oscillations. Furthermore, we have transformed the coordinate from (E_r, E) to (E_{bias}, E_c) using the following equation (2) [10] and plotted the distribution of ρ^- versus built-in-bias field E_{bias} and coercive field E_c as shown in Fig. 4 (a-c).

$$E_{bias} = \frac{E + E_r}{2} \ , \ E_C = \frac{E - E_r}{2} \qquad (2)$$

The E_c distributes from 4.14 MV/cm to 4.54 MV/cm (Fig. 4a), 4.16 MV/cm to 4.68 MV/cm (Fig. 4b), and 4.25 MV/cm to 4.95 MV/cm (Fig. 4c) for 50 nm, 40 nm, and 30 nm $Al_{0.7}Sc_{0.3}N$ films respectively. The corresponding $|E_{bias}|$ is around 0.34 MV/cm, 0.35 MV/cm, and 0.37 MV/cm respectively. It is clearly seen that coercive field E_c increases [Fig. 4d] and is distributed more widely with decreased $Al_{0.7}Sc_{0.3}N$ film thickness. However, the switching density ρ^- decreases with a decrease in ferroelectric $Al_{0.7}Sc_{0.3}N$ film thickness. A reduction of ρ^- in thinner $Al_{0.7}Sc_{0.3}N$ films is more likely because of wider distribution of E_c. The increased E_c for thinner $Al_{0.7}Sc_{0.3}N$ films has been attributed to the effect of an adjacent interfacial layer near the electrodes or to the additional pinning of domain walls in thinner ferroelectric films. On the other hand, in a built-in-bias field, E_{bias} distribution becomes wider, and $|E_{bias}|$ increases slightly in thinner $Al_{0.7}Sc_{0.3}N$ films as shown in Fig.4d.

IV. CONCLUSIONS

In this work, $Al_{0.7}Sc_{0.3}N$ ferroelectric film thickness-dependent switching characteristics have been experimentally demonstrated in Mo/$Al_{0.7}Sc_{0.3}N$/Mo MFM capacitors by employing the FORC approach. FORC analysis shows the impact of ferroelectric film thickness on the switching density ρ^-, coercive field E_c, reversal field E_r, and built-in-bias field E_{bias} distributions. Our experimental results exhibit that ρ^- decreases while $|E_r|$ and E_c increase with scaling down $Al_{0.7}Sc_{0.3}N$ film thickness to 30 nm. This insightful study may help to understand the effect of $Al_{0.7}Sc_{0.3}N$ film thickness on ferroelectric switching for future NVM applications.

ACKNOWLEDGEMENT

This work was supported by the Science and Engineering Research Council of A*STAR (Agency for Science, Technology and Research) Singapore, under Grant No. A20G9b0135.

REFERENCES

[1] T. Mikolajick, S. Slesazeck, H. Mulaosmanovic, M. H. Park, S. Fichtner, P. D. Lomenzo, M. Hoffmann, and U. Schroeder, "Next generation ferroelectric materials for semiconductor process integration and their applications," *J. Appl. Phys*., vol. 129, pp. 100901, 2021. doi: 10.1063/5.0037617

[2] S. Fichtner, N. Wolff, F. Lofink, L. Kienle, and B. Wagner, "AlScN: A III-V semiconductor based ferroelectric," *J. Appl. Phys*., vol. 125, pp. 114103, 2019. doi: 10.1063/1.5084945

[3] C. Liu, Q. Wang, W. Yang, T. Cao, L. Chen, M. Li, F. Liu, D.K. Loke, J. Kang, and Y. Zhu, "Multiscale Modeling of $Al_{0.7}Sc_{0.3}N$-based FeRAM: the steep switching, leakage and selector-free array," 2021 *IEEE International Electron Devices Meeting (IEDM)*, pp. 8.1.1-8.1.4, 2021. doi: 10.1109/IEDM19574.2021.9720535

[4] L. Chen, C. Liu, M. Li, W. Song, W. Wang, Z. Chen, S. Samanta, H. K. Lee, and Y. Zhu, "Bipolar and unipolar cycling behavior in ferroelectric scandium-doped aluminum nitride," *2022 IEEE International Symposium on Applications of Ferroelectrics (ISAF)*, 2022. doi: 10.1109/ISAF51494.2022.9870042

[5] S. Chen, K. Han, S. Samanta, Q. Kong, J. Zhang, H. Xu, W. Xinke, A. Kumar, C. Wang, Z. Zijie, Y. Xunzhao, K. Ni, X. Gong, "First demonstration of BEOL-compatible ferroelectric TCAM featuring a-IGZO Fe-TFTs with large memory window of 2.9 V, scaled channel length of 40 nm, and high endurance of 10^8 cycles," *2021 IEEE Symposium on VLSI Technology*, T7-4, 2021.

[6] H. Sun, Z. Luo, C. Liu, C. Ma, Z. Wang, Y. Yin, and X. Li, "A flexible $BiFeO_3$-based ferroelectric tunnel junction memristor for neuromorphic computing," *J. Materiomics*, vol. 8, pp. 144-149, 2022. doi: 10.1016/j.jmat.2021.04.009

[7] C. Besleaga, R. Radu, L. M. Balescu, V. Stancu, A. Costas, V. Dumitru, G. Stan, and L. Pintilie, " Ferroelectric field effect transistor based on PZT and IGZO," *IEEE J. Electron Dev. Soc*., vol. 7, pp. 268-275, 2019. doi: 10.1109/JEDS.2019.2895367

[8] S. Yasuoka, T. Shimizu, A. Tateyama, M. Uehara, H. Yamada, M. Akiyama, Y. Hiranaga, Y. Cho, and H. Funakubo, "Effects of deposition conditions on the ferroelectric properties of $(Al_{1-x}Sc_x)N$ thin films," *J. Appl. Phys*., vol. 128, pp. 114103, 2020. doi: 10.1063/5.0015281

[9] J. X. Zheng, M. M. A. Fiagbenu, G. Esteves, P. Musavigharavi, A. Gunda, D. Jariwala, E. A. Stach, and R. H. Olsson III, " Ferroelectric behavior of sputter deposited $Al_{0.72}Sc_{0.28}N$ approaching 5 nm thickness," *Appl. Phys. Lett*., vol. 122, pp. 222901, 2023. doi: 10.1063/5.0147224

[10] T. Schenk, M. Hoffmann, J. Ocker, M. Pesic, T. Mikolajick, and U. Schroeder, "Complex internal bias fields in ferroelectric hafnium oxide," *ACS Appl. Mater. Interfaces*, vol. 7, pp. 20224-20233, 2015. doi: 10.1021/acsami.5b05773.